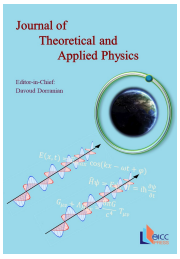

Volume 17, Issue 1, 172306 (1-6)

Journal of Theoretical and Applied Physics (JTAP)

https://dx.doi.org/10.57647/j.jtap.2023.1701.06

Optimizing electron trajectories in combined helical wiggler and solenoidal magnetic fields for effective particle acceleration

Hitendra K. Malik*

Plasma Science and Technology Laboratory, Department of Physics, Indian Institute of Technology Delhi, New Delhi, India.

***Corresponding author**: hkmalik@physics.iitd.ac.in

Received 30 September 2022; Accepted 8 November 2022; Published online 15 November 2022

Abstract:
Charged particle acceleration is the subject of great interest because of its applications in various fields such as thermonuclear fusion, nuclear physics, radiation generation, coherent harmonic generation, probing materials, medical science, food preservation, etc. The particle acceleration is usually done by interacting the particles with strong electric fields. Since the magnetic field diverts the particle motion, this also plays a vital role in the particle interaction with the electromagnetic fields. In the present work, a combined configuration of helical wiggler and solenoidal magnetic fields has been used to optimize the trajectory of the electron for effective particle acceleration. In this concept, the solenoidal field controls the transverse components of the electron velocities and wiggler field confines the helical motion of the electron. The optimized values of magnitudes of solenoidal field and wiggler magnetic field and its period / wavelength make this configuration useful for particle acceleration in waveguide.

Keywords: Solenoidal magnetic field; Helical Wiggler magnetic field; Electron trajectories; Larmor radius; Pitch

1. Introduction

Several schemes have been developed in laboratories for charged particle acceleration and to achieve a high-quality beam of such particles [1–9]. The particles have been found to accelerate by the shocks [10]; even the acceleration of galactic cosmic rays is accounted by the shocks emanating from supernova explosions and propagating through the interstellar medium [11]. In laboratory / computer simulations also, the use of shocks has been made to accelerate the particles [10]. The recent acceleration techniques involve photonic chip-based particle acceleration [12], relativistic reconnection [13], bubble acceleration [14], etc. In most of the schemes, this can be seen that the laser beams have been largely used for the purpose of particle acceleration and very sophisticated equipment are required. However, the microwave pulses with special shapes have proved their effectiveness while being used in the plasma-filled waveguides [8, 15, 16]. In such mechanisms, the magnetic field has been employed for the extraction of accelerated particles [17]. Not only this, but the magnetic field is also found to control the radiation emission and to enhance the efficiency of the schemes [18–20].

In the mechanisms of particle acceleration and the radiation generation, the electron motion or its trajectory needs to be controlled as it plays a vital role for the effective interaction of the electron with the electromagnetic field. The calculations for the electron trajectories in free electron laser (FEL) with helical wiggler and axial guide fields has been done by several researchers [21–24]. For example, Aamodt [21] has calculated the expressions for the electron orbits analytically in the presence of a longitudinal wiggler magnetic field. Freund and Ganguly [22] have developed a theory for non-steady trajectories in three-dimensional helical wiggler magnetic field. Fajans et al. [23] have analyzed off axis electron orbits in FEL beam in the presence of combination of helical wiggler and axial guide field. El-Bahi et al. [24] have described the electron trajectories in helical free electron laser. On the other hand, Punia and Malik [25] have used the combined configuration of helical wiggler and solenoidal magnetic fields to generate polarization-tunable terahertz radiation. Recently, three-coil set ups with rectangular cross

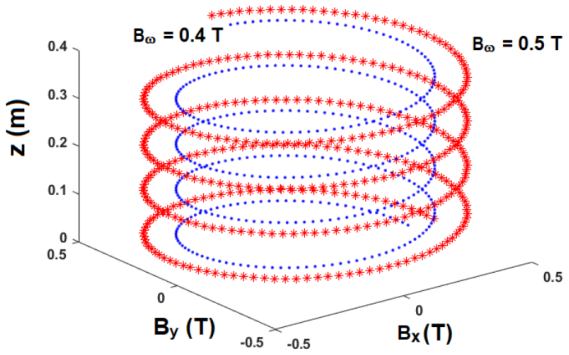

Figure 1. Profile of the helical wiggler magnetic field for different values of B_ω, when $\delta_\omega = 2/3\times10^2$ m^{-1}.

section coils [26] or tapered coils [27] have been proposed to control the magnetic field topology in a magnetic nozzle, which is a device for space propulsion. Since the separation of electrons from the ions in these devices take place due to the magnetic field distribution, the electron motion here played an important role in creating the ambipolar field and hence, in controlling the thrust. In the present letter, considering the combined configuration of helical wiggler and solenoidal magnetic fields, the expressions for the electron velocity components have been derived analytically and the relevant equations are solved numerically in MATLAB using fourth-order Runge-Kutta method (ODE45) for investigating the electron trajectories under different injection positions of the electron. The optimization of the same is expected to produce effective electron acceleration when it is subjected to the electromagnetic field of the microwaves.

2. Mathematical equations

A combined configuration of solenoidal and wiggler magnetic fields is considered in the present work, with the following expression

$$B = B_s\hat{z} + B_\omega[\cos(\delta_\omega z\hat{x}) + \sin(\delta_\omega z\hat{y})] \tag{1}$$

Here δ_ω is the wave number corresponding to the wavelength λ_ω of the wiggler magnetic field, given as $\delta_\omega = 2\pi/\lambda_\omega$. B_ω is the peak value of the helical wiggler field and B_s is the magnitude of the solenoidal field. The solenoidal field has been applied in the z direction, so it will provide a circular motion to the electron and control the transverse (x and y) components of its velocity. The wiggler field is circularly polarised in nature and it will rotate around z axis as the advancement in z results in a helical magnetic field (Figure 1). So, this field is expected to provide helical motion to the electron with higher acceleration if the electron is subjected to external electric field. It can be seen from Figure 1 that the diameter of the circle is enhanced when the peak value of the wiggler field is increased from 0.4 T to 0.5 T. On the other hand, the periodicity or the wavelength of the field decreases with the increasing values of δ_ω (please see Figure 2, where the graph marked with red stars corresponds to δ_ω = 300/3 m^{-1} and the graph with blue dots corresponds to δ_ω = 200/3 m^{-1}. The addition of the solenoidal field increases the peak value of the combined

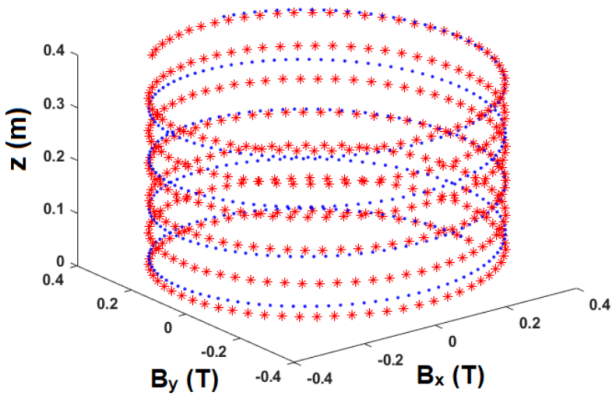

Figure 2. Profile of the helical wiggler magnetic field for different values of δ_ω (δ_ω = 300/3 m^{-1} for the graph marked with red stars and δ_ω = 200/3 m^{-1} for the graph marked with blue dots), when B_ω = 0.4 T.

magnetic field, as shown in Figure 3.
The equation of motion for the electron under the said configuration of the magnetic field is written as

$$m\frac{d\mathbf{v}}{dt} = -e(\mathbf{v}\times\mathbf{B}) \tag{2}$$

Here $\mathbf{v} = v_x\hat{x} + v_y\hat{y} + v_z\hat{z}$ is the velocity of the electron, -e is the electronic charge and m is the mass of the electron. Equations (1) and (2) result in the following set of three equations:

$$\frac{dv_x}{dt} = -\frac{e}{m}[v_yB_s - v_zB_\omega\sin(\delta_\omega z)] \tag{3}$$

$$\frac{dv_y}{dt} = -\frac{e}{m}[v_zB_\omega\cos(\delta_\omega z) - v_xB_s] \tag{4}$$

$$\frac{dv_z}{dt} = -\frac{e}{m}[v_xB_\omega\sin(\delta_\omega z) - v_yB_\omega\cos(\delta_\omega z)] \tag{5}$$

These equations have been solved by taking three different sets of initial conditions to get the velocity components in each case. Assuming that the electron enters in the magnetic

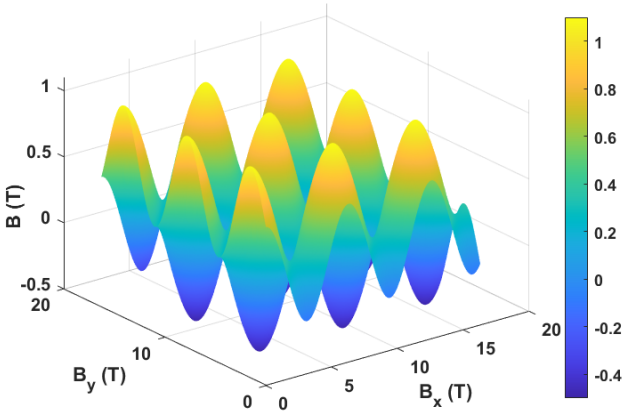

Figure 3. Profile of the combined magnetic field having solenoidal (B_S = 0.3 T) and helical wiggler (B_ω = 0.4 T) magnetic fields.

field (at $t = 0$) with the initial velocity in x-y plane from the origin and $v_x(t = 0)= v_{x0}$, $v_y(t = 0)= v_{y0}$, $v_z(t = 0)= 0$, we get

$$v_x = \left\{ \begin{array}{c} v_{x0}\frac{B_\omega^2}{B_s^2+2B_\omega^2}+ \\ \\ v_{x0}\frac{B_s+B_\omega^2}{B_s^2+2B_\omega^2}\cos(\frac{e}{m}\sqrt{B_s^2+B_\omega^2}t)+ \\ \\ v_{y0}\frac{B_s}{\sqrt{B_s^2+B_\omega^2}}\sin(\frac{e}{m}\sqrt{B_s^2+B_\omega^2}t) \end{array} \right\} \tag{6}$$

$$v_y = v_{x0}\frac{\tan(\delta_\omega z)B_\omega^2}{B_s^2+2B_\omega^2}+$$

$$\cos(\frac{e}{m}\sqrt{B_s^2+B_\omega^2}t)\times\left\{ \begin{array}{c} v_{y0}\frac{B_s^2}{B_s^2+B_\omega^2[\sin(\delta_\omega z)]^2}- \\ \\ \frac{v_{x0}}{2}\frac{(B_s^2+B_\omega^2)B_\omega^2\sin(2\delta_\omega z)}{(B_s^2+B_\omega^2)(B_s^2+B_\omega^2[\sin(\delta_\omega z)]^2)} \end{array} \right\}+$$

$$\sin(\frac{e}{m}\sqrt{B_s^2+B_\omega^2}t)\times\left\{ \begin{array}{c} v_{y0}\frac{B_s^2B_\omega^2\sin(2\delta_\omega z)}{2\sqrt{B_s^2+B_\omega^2}(B_s^2+B_\omega^2[\sin(\delta_\omega z)]^2)}+ \\ \\ v_{x0}\frac{B_s(B_s^2+B_\omega^2)^{\frac{3}{2}}}{(B_s^2+2B_\omega^2)(B_s^2+B_\omega^2[\sin(\delta_\omega z)]^2)} \end{array} \right\} \tag{7}$$

$$v_z = v_{x0}\frac{B_\omega^2B_s\sec(\delta_\omega z)}{B_s^2+2B_\omega^2}-$$

$$\cos(\frac{e}{m}\sqrt{B_s^2+B_\omega^2}t)\times\left\{ \begin{array}{c} v_{x0}\frac{B_\omega^2B_s(B_s^2+B_\omega^2)\cos(\delta_\omega z)}{(B_s^2+2B_\omega^2)(B_s^2+B_\omega^2[\cos(\delta_\omega z)]^2)}+ \\ \\ v_{y0}\frac{B_\omega^2B_s\sin(\delta_\omega z)}{(B_s^2+B_\omega^2[\cos(\delta_\omega z)]^2)} \end{array} \right\}+$$

$$\sin(\frac{e}{m}\sqrt{B_s^2+B_\omega^2}t)\times\left\{ \begin{array}{c} v_{y0}\frac{B_\omega B_s^2\cos(\delta_\omega z)}{\sqrt{B_s^2+B_\omega^2}(B_s^2+B_\omega^2[\cos(\delta_\omega z)]^2)}- \\ \\ v_{x0}\frac{B_\omega(B_s^2+B_\omega^2)^{\frac{3}{2}}\sin(\delta_\omega z)}{(B_s^2+2B_\omega^2)(B_s^2+B_\omega^2[\cos(\delta_\omega z)]^2)} \end{array} \right\} \tag{8}$$

For the case the electron enters in the magnetic field (at $t = 0$) with initial velocity in y-z plane from the origin and v_x ($t = 0$)$= 0$, v_y ($t = 0$)$= v_{y0}$, v_z ($t = 0$)$= v_{z0}$, we get

$$v_x = \left\{ \begin{array}{c} v_{z0}\frac{B_s(B_s^2+2B_\omega^2)}{B_\omega(B_s^2+B_\omega^2)}- \\ \\ v_{z0}\frac{B_s(B_s^2+2B_\omega^2)}{B_\omega(B_s^2+B_\omega^2)}\cos(\frac{e}{m}\sqrt{B_s^2+B_\omega^2}t)+ \\ \\ v_{y0}\frac{B_s}{\sqrt{B_s^2+B_\omega^2}}\sin(\frac{e}{m}\sqrt{B_s^2+B_\omega^2}t) \end{array} \right\} \tag{9}$$

$$v_y = v_{z0}\frac{B_s(B_s^2+2B_\omega^2)}{B_\omega(B_s^2+B_\omega^2)}\tan(\delta_\omega z)+$$

$$\cos(\frac{e}{m}\sqrt{B_s^2+B_\omega^2}t)\times\left\{ \begin{array}{c} v_{z0}\frac{B_\omega B_s(B_s^2+2B_\omega^2)\sin(2\delta_\omega z)}{2(B_s^2+B_\omega^2)(B_s^2+B_\omega^2[\sin(\delta_\omega z)]^2)}+ \\ \\ v_{y0}\frac{B_s^2}{(B_s^2+B_\omega^2[\sin(\delta_\omega z)]^2)} \end{array} \right\}+$$

$$\sin(\frac{e}{m}\sqrt{B_s^2+B_\omega^2}t)\times\left\{ \begin{array}{c} v_{y0}\frac{B_sB_\omega^2\sin(2\delta_\omega z)}{2\sqrt{B_s^2+B_\omega^2}(B_s^2+B_\omega^2[\sin(\delta_\omega z)]^2)}- \\ \\ v_{z0}\frac{B_s^2(B_s^2+B_\omega^2)}{B_\omega\sqrt{B_s^2+B_\omega^2}(B_s^2+B_\omega^2[\sin(\delta_\omega z)]^2)} \end{array} \right\} \tag{10}$$

$$v_z = v_{z0}\frac{B_s^2(B_s^2+2B_\omega^2)}{B_\omega^2(B_s^2+B_\omega^2)}\sec(\delta_\omega z)+$$

$$\cos(\frac{e}{m}\sqrt{B_s^2+B_\omega^2}t)\times\left\{ \begin{array}{c} v_{z0}\frac{B_s^2(B_s^2+2B_\omega^2)\cos(\delta_\omega z)}{(B_s^2+B_\omega^2)(B_s^2+B_\omega^2[\cos(\delta_\omega z)]^2)}- \\ \\ v_{y0}\frac{B_\omega B_s\sin(\delta_\omega z)}{(B_s^2+B_\omega^2[\cos(\delta_\omega z)]^2)} \end{array} \right\}+$$

$$\sin(\frac{e}{m}\sqrt{B_s^2+B_\omega^2}t)\times\left\{ \begin{array}{c} v_{y0}\frac{B_\omega B_s^2\cos(\delta_\omega z)}{\sqrt{B_s^2+B_\omega^2}(B_s^2+B_\omega^2[\cos(\delta_\omega z)]^2)}+ \\ \\ v_{z0}\frac{B_\omega B_s\cos(\delta_\omega z)}{\sqrt{B_s^2+B_\omega^2}(B_s^2+B_\omega^2[\cos(\delta_\omega z)]^2)} \end{array} \right\} \tag{11}$$

When the electron enters in the magnetic field (at $t = 0$) with initial velocity in z-x plane from the origin and v_x ($t = 0$)$= v_{x0}$, v_y ($t = 0$)$= 0$, v_z ($t = 0$)$= v_{z0}$, we get

$$v_x = \left\{ \begin{array}{c} v_{x0}\frac{B_\omega^2}{(B_s^2+2B_\omega^2)}+v_{z0}\frac{B_\omega(B_s^2+B_\omega^2)}{B_s(B_s^2+2B_\omega^2)}+ \\ \\ \cos(\frac{e}{m}\sqrt{B_s^2+B_\omega^2}t)\times\left[v_{x0}\frac{(B_s^2+B_\omega^2)}{(B_s^2+2B_\omega^2)}-v_{z0}\frac{B_\omega(B_s^2+B_\omega^2)}{B_s(B_s^2+2B_\omega^2)}\right] \end{array} \right\} \tag{12}$$

$$v_y = \tan(\delta_\omega z)\left[v_{x0}\frac{B_\omega^2}{(B_s^2+2B_\omega^2)}+v_{z0}\frac{B_\omega(B_s^2+B_\omega^2)}{B_s(B_s^2+2B_\omega^2)}\right]+$$

$$\left[v_{x0}\frac{(B_s^2+B_\omega^2)}{(B_s^2+2B_\omega^2)}-v_{z0}\frac{B_\omega(B_s^2+B_\omega^2)}{B_s(B_s^2+2B_\omega^2)}\right]\times$$

$$\left\{ \begin{array}{c} \cos(\frac{e}{m}\sqrt{B_s^2+B_\omega^2}t)\frac{-B_\omega^2\sin(2\delta_\omega z)}{2(B_s^2+B_\omega^2[\sin(\delta_\omega z)]^2)}+ \\ \\ \sin(\frac{e}{m}\sqrt{B_s^2+B_\omega^2}t)\frac{B_s\sqrt{B_s^2+B_\omega^2}}{(B_s^2+B_\omega^2[\sin(\delta_\omega z)]^2)} \end{array} \right\} \tag{13}$$

$$v_z = \frac{B_s}{B_\omega(B_s^2+2B_\omega^2)}\sec(\delta_\omega z)\left[v_{x0}B_\omega^2+v_{z0}\frac{B_\omega(B_s^2+B_\omega^2)}{B_s}\right]-$$

$$(v_{x0}-v_{z0}\frac{B_\omega}{B_s})\times\left\{ \begin{array}{c} \cos(\frac{e}{m}\sqrt{B_s^2+B_\omega^2}t)\times \\ \\ \frac{B_\omega B_s(B_s^2+B_\omega^2)}{(B_s^2+2B_\omega^2)(B_s^2+B_\omega^2[\cos(\delta_\omega z)]^2)} \end{array} \right\}+$$

$$(v_{x0}-v_{z0}\frac{B_\omega}{B_s})\times\left\{ \begin{array}{c} \sin(\frac{e}{m}\sqrt{B_s^2+B_\omega^2}t)\times \\ \\ \frac{B_\omega(B_s^2+B_\omega^2)^{\frac{3}{2}}\sin(\delta_\omega z)}{(B_s^2+2B_\omega^2)(B_s^2+B_\omega^2[\cos(\delta_\omega z)]^2)} \end{array} \right\} \tag{14}$$

3. Results and discussion

The effect of magnitudes of the solenoidal and wiggler magnetic fields is analysed in greater detail in this section by taking their different values and then comparing the electron trajectories in both the cases. This comparison enables us to get the controlling parameters for the trajectory. This effect has been analysed by considering three sets of different initial conditions.

3.1 Electron injection in x-y plane

The particle enters the interaction region initially having velocity 0.2c in the x- and y- directions (x-y plane). The electron trajectory obtained numerically [28–31] based on the equations (6) – (8) is shown in Figure 4. Since both the velocity of electron and helical wiggler field are in the

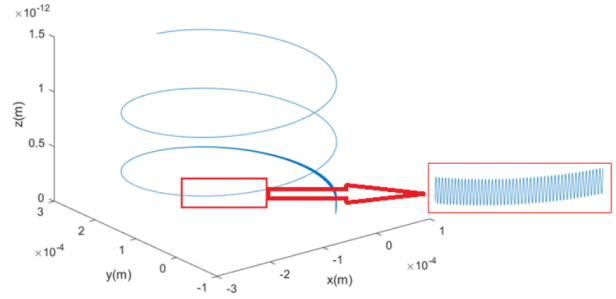

Figure 4. Trajectory of electron when $v_{x0} = v_{y0} = 0.2c$, $v_{z0} = 0$, $\delta_\omega = 2/3\times10^2$ m^{-1}, and $B_s = B_\omega = 0.3$ T.

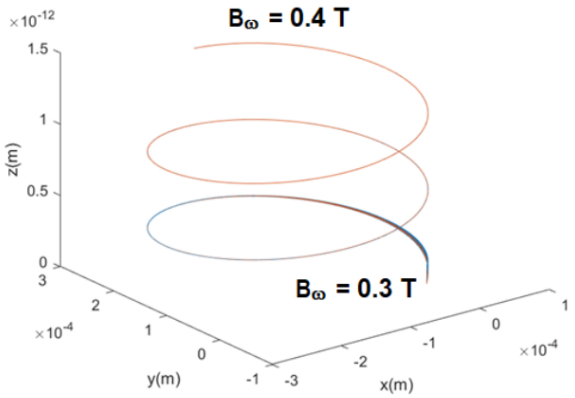

Figure 6. Effect of wiggler magnetic field on trajectory when $v_{x0} = v_{y0} = 0.2c$, $v_{z0} = 0$, $\delta_\omega = 2/3\times10^2$ m^{-1}, and $B_s = 0.3$ T.

x-y plane in this case but the solenoidal field is in the z-direction, the solenoidal field causes the electron to move in a circular path only. On the other hand, the wiggler field's y-component alters the x-component of the velocity and produces sinusoidal oscillations in the x-z plane. The x-component of the field alters the y-component of the velocity and produces sinusoidal oscillations in the y-z plane. The sinusoidal oscillations are shown in the inset of the figure. Here the helical nature of the field also causes the electron to move in the helical path.

If we look at the role of the solenoidal field (B_s), the radius of the trajectory is found to decrease with the increase in the strength of this field (Figure 5). This can be understood based on the relation of the Larmor radius and the magnetic field, i.e. $r = mv/eB_s$, where v is the perpendicular component of the velocity of the electron. However, the enhancement of the magnitude of the wiggler magnetic field (B_ω) causes no change in the radius of the trajectory, as the radius in this case is independent of B_ω. Hence, both the graphs in Figure 6 overlap each other for the two values of B_ω as 0.3 T and 0.4 T.

3.2 Electron injection in y-z plane

Now we discuss the case where the electron enters the interaction region initially having velocity 0.2c in the y- and z-directions. For this, we need to solve the set of equations (9) – (11) to find the x-, y-, and z-coordinates for evaluating the electron trajectory. The results are shown in Figure 7.

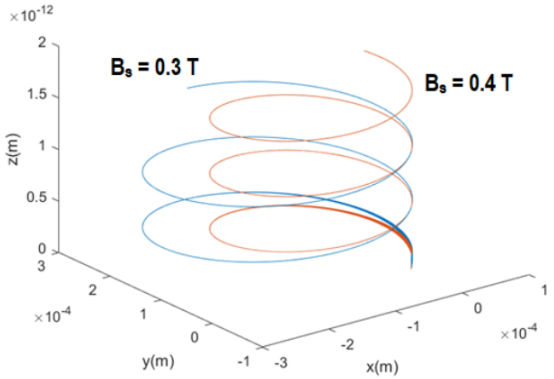

Figure 5. Effect of solenoidal field on trajectory when $v_{x0} = v_{y0} = 0.2c$, $v_{z0} = 0$, $\delta_\omega = 2/3\times10^2$ m^{-1}, and $B_\omega = 0.3$ T.

Since the electron is injected in the y-z plane having velocity components in the x- and z-directions, the solenoidal field (due to Lorentz force) causes the helical motion. As the wiggler field and velocity components are lying in different directions, the wiggler field also contributes to the radius of the electron motion trajectory in this case as well as in the helical motion. The Larmor radius is found to decrease with the increasing strength of the solenoidal field (Figure 7). While this time radius is dependent on the wiggler magnetic field too, so on changing B_ω the radius of the motion also changes. Please see this result in Figure 8. An increase in the magnitude of wiggler field increases the radius of the helix of helical wiggler field due to which the radius of trajectory also increases. This is due to the combined effect of the two fields.

3.3 Electron injection in x-z plane

Finally, we consider the situation where the electron enters the interaction region initially having velocity 0.2c in the x- and z-directions, i.e., the x-z plane. For this case, we need to solve the set of equations (12) – (14). The resultant

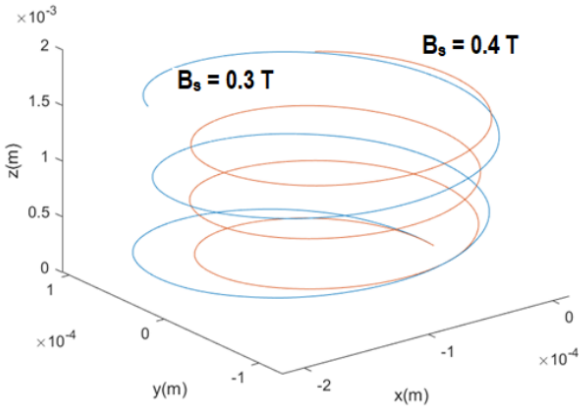

Figure 7. Effect of solenoidal field on the trajectory when $v_{y0} = v_{z0} = 0.2c$, $v_{x0} = 0$, $\delta_\omega = 2/3\times10^2$ m^{-1}, and $B_\omega = 0.3$ T.

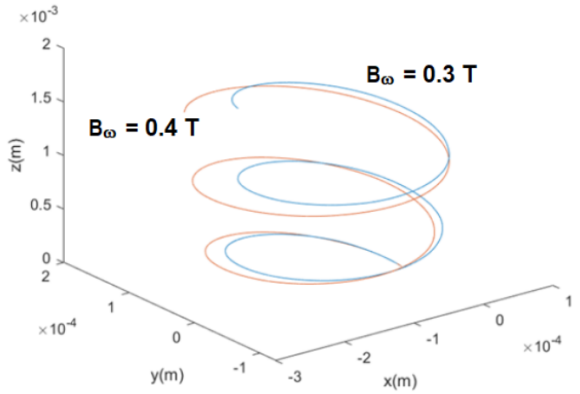

Figure 8. Effect of wiggler field on trajectory when v_{y0} = v_{z0} = 0.2c, v_{x0} = 0, δ_ω = 2/3×10^2 m^{-1}, and B_s = 0.3 T.

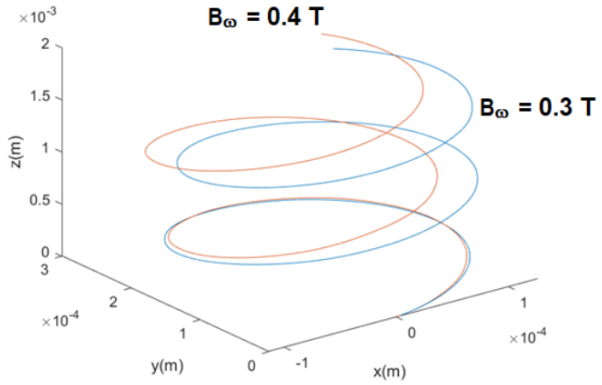

Figure 10. Effect of wiggler field on trajectory when v_{x0} = v_{z0} = 0.2c, v_{y0} = 0, δ_ω = 2/3×10^2 m^{-1}, and B_s = 0.3 T.

electron trajectory is shown in Figure 9. Due to v_x and v_y components, the solenoidal field (applied in the z-direction) contributes to the helical motion of the electron. Similar to the previous case, the wiggler field and velocity are in different directions (planes), so the wiggler field contributes to the radius of the motion as well as to the helical motion (circular polarisation of the wiggler field). Under this situation, larger the solenoidal field is, smaller is the radius of the trajectory helix (please see Figure 9). On the other hand, the radius of the helical path is also found to change with the change in the wiggler field B_ω; this is evident from Figure 10.

Finally, we discuss the situation of relativistic speed of the electron when it is launched in the said configuration of magnetic field. The present calculations were carried out by neglecting the relativistic effects. However, there will be a variation in the electron mass when it propagates at the relativistic speed that will modify the cyclotron frequency. Also, the relativistic factor is expected to appear in the calculations and it will become more complicated to separate out all the velocity components in the methodology we developed under the effect of combined solenoidal and helical-wiggler magnetic fields. With regard to achieving

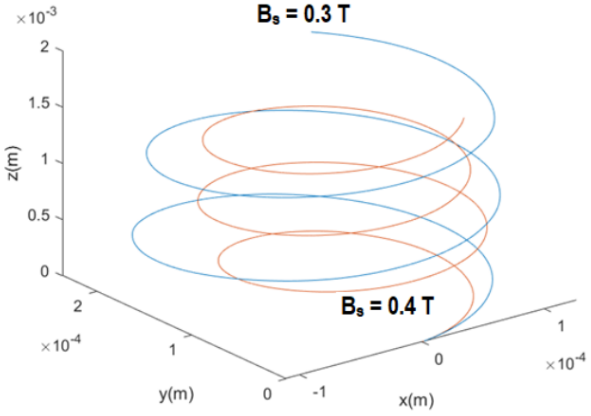

Figure 9. Effect of solenoidal field on trajectory when v_{x0} = v_{z0} = 0.2c, v_{y0} = 0, δ_ω = 2/3×10^2 m^{-1}, and B_ω = 0.3 T.

the said magnetic field, we mention that a transverse periodic helical magnetic field can be produced on the axis of a double-helix-wound bifilar magnet with equal and opposite currents in each helix [32]. Helical magnetic field has been produced during preheating at the electroweak scale [33]. When the transverse and constant magnetic field rotates in helical fashion the field is called helical-wiggler magnetic field. Wiggler magnetic field with exponential entrance has been produced using the permanent magnets and aluminium holders [34].

4. Conclusion

Different cases were discussed for the electron trajectory under the impact of combined solenoidal magnetic field applied along the z-direction and wiggler magnetic field applied in the x-y plane. A comparison of the electron trajectories under various initial conditions and the magnitudes of both kinds of the magnetic fields enables one to optimize the parameters to control the motion of the electron. The radius of trajectory decreases with increasing strength of the solenoidal field, controlling the transverse components of the electron velocity. For its magnitude of 0.3 T and the electron initial velocity as 6×10^6 m/s, the radius of motion is of the order of 10^{-4} m, while the pitch is of the order of 10^{-3} m. At the entrance of the wiggler, some fraction of axial velocity (z-component) is found to be converted into perpendicular velocity by the wiggler, resulting in the helical trajectory of the electron. The interaction time between the electron and the field is increased by using the helical wiggler magnetic field, which is expected to help providing the electron more intense acceleration in the presence of external electric field. The configuration proposed in this article can be used in a rectangular waveguide for electron acceleration using microwaves, where the radius of circular motion is controlled by the solenoidal field and the helical motion is confined by the wiggler field. This is in view of the fact that the magnetic fields with periodicity / wavelength in centimeters or fraction in centimeters can be easily produced and the wavelength of the microwaves also lies in centimeters. Also by filling this waveguide with plasma, one can additionally control the cutoff frequency and

interaction length for achieving the resonance and effective particle acceleration.

Conflict of interest statement
The authors declare that they have no conflict of interest.

References

[1] H. K. Malik. *Laser-Matter Interaction for Radiation and Energy*. CRC Press, 1th edition, 2021.

[2] H. K. Malik, S. Kumar, and K. PSingh. *Laser and Particle Beams*, **26**:197, 2008.

[3] S. Kumar and H. K. Malik. *Journal of plasma physics*, **72**:983, 2006.

[4] H. K. Malik, S. Kumar, V. Dhaka, and D. K. Singh. *Journal of Theoretical and Applied Physics*, **15**:1, 2021.

[5] H. K. Malik. *Plasma Science and Technology*, **6**:2456, 2004.

[6] S. Kumar, D. N. Gupta, H. K. Malik, D. Singh, J. Lee, and M. Yoon. *Physics of Plasmas*, **27**:043105, 2020.

[7] M. Yadav, D. N. Gupta, and S. C. Sharma. *Physics of Plasmas*, **27**:093106, 2020.

[8] H. K. Malik. *Journal of applied physics*, **104**:053308, 2008.

[9] L. Comisso and L. Sironi. . *Physical Review Letters*, **127**:255102, 2021.

[10] R. B. Decker. *Space Science Reviews*, **48**:195, 1988.

[11] R. D. Blandford and J. P. Ostriker. *The Astrophysical Journal*, **221**:L29, 1978.

[12] R. Shiloh, J. Illmer, T. Chlouba, P. Yousefi, N. Schönenberger, U. Niedermayer, A. Mittelbach, and P. Hommelhoff. *Nature*, **597**:498, 2021.

[13] H. Zhang, L. Sironi, and D. Giannios. *The Astrophysical Journal*, **922**:261, 2021.

[14] Z. Ren, Z. Zuo, S.Wu, and S. Liu. *Physical Review Letters*, **128**:044501, 2022.

[15] H. K. Malik. *Journal of plasma physics*, **69**:59, 2003.

[16] A. K. Aria, H. K. Malik, and K. P. Singh. *Laser and Particle Beams*, **27**:41, 2009.

[17] H. K. Malik. *Journal of plasma physics*, **68**:211, 2002.

[18] H. K. Malik and S. Punia. *Physics of Plasmas*, **26**:063102, 2019.

[19] H. K. Malik. *Physics Letters A*, **379**:2826, 2015.

[20] B. Bernáth, P. Gogoi, A. Marchese, D. Kamenskyi, H. Engelkamp, D. Arslanov, B. Redlich, P. C. Christianen, and J. C. Maan. *Physical Review B*, **105**:205204, 2022.

[21] R. E. Aamodt. *Physical Review A*, **28**:2895, 1983.

[22] H. Freund and A. Ganguly. *IEEE journal of quantum electronics*, **21**:1073, 1985.

[23] J. Fajans, D. A. Kirkpatrick, and G. Bekefi. *Physical Review A*, **32**:3448, 1985.

[24] R. El-Bahi, M. N. Rhimi, and A. W. Cheikhrouhou. *Brazilian Journal of Physics*, **32**:790, 2002.

[25] S. Punia and H. K. Malik. *Plasma Sources Science and Technology*, **28**:115018, 2019.

[26] L. Malik, M. Kumar, and I. V. Singh. *IEEE Transactions on Plasma Science*, **49**:2227, 2021.

[27] L. Malik. *Propulsion and Power Research*, **11**:171, 2022.

[28] L. Malik and A. Tevatia. *Defence Science Journal*, **71**:1, 2021.

[29] L. Malik, S. Rawat, M. Kumar, and A. Tevatia. *Physics Review D*, **102**:036020, 2021.

[30] L. Malik, A. Escarguel, M. Kumar, A. Tevatia, and R. S. Sirohi. *Laser Physics Letters*, **18**:086003, 2021.

[31] L. Malik. *Optics and Laser Technology*, **132**:106485, 2020.

[32] B. M. Kincaid. *Journal of Applied Physics*, **48**:2684, 1977.

[33] A. Diaz-Gil, J. Garcia-Bellido, M. G. Perez, and A. Gonzalez-Arroyo. *Physical Review Letters*, **100**:241301, 2008.

[34] A. Al-Shamma, R. A. Stuart, and J. Lucas. *Nuclear Instruments and Methods in Physics Research Section A: Accelerators, Spectrometers, Detectors and Associated Equipment*, **375**:424, 1996.